



# LUND UNIVERSITY

Department of Water Resources Engineering

---

## LUP

Lund University Publications  
Institutional Repository of Lund University  
Found at: <http://www.lu.se>

This is an author produced version of a paper published in  
Journal of Hydraulic Engineering

This paper has been peer-reviewed but does not include the  
final publisher proof-corrections or journal pagination.

Citation for the published paper:

Authors: Charlotta Borell Lövestedt, Magnus Larson

Title: Wave Damping in Reed : Field Measurements and  
Mathematical Modeling

Journal: Journal of Hydraulic Engineering, 2010, Vol. 136,  
Issue: 4, pp: 222-234

DOI: [http://dx.doi.org/10.1061/\(ASCE\)HY.1943-7900.0000167](http://dx.doi.org/10.1061/(ASCE)HY.1943-7900.0000167)

Access to the published version may  
require subscription.

Published with permission from: ASCE

# Wave Damping in Reed:

## Field Measurements and Mathematical Modeling

Charlotta Borell Lövestedt<sup>1</sup> and Magnus Larson<sup>2</sup>

### Abstract

Wave damping in vegetation in shallow lakes reduces resuspension and thereby improves the light climate and decreases nutrient recycling. In this study, wave transformation in reed (*Phragmites australis*) was measured in a shallow lake. Theoretical models of wave height decay, based on linear wave theory, and transformation of the probability density function, using a wave-by-wave approach, were developed and compared to the collected data. Field data showed an average decrease in wave height of 4–5% m<sup>-1</sup> within the first 5–14 m of the vegetation. Incident root-mean-square wave height varied between 1 and 8 cm, which is typical for the studied lake. A species-specific drag coefficient,  $C_D$ , was found to be about 9 (most probable range: 3–25), and the model was relatively insensitive to moderate variations in this parameter. The coefficient showed little correlation with a Reynolds number or a Keulegan-Carpenter number. The probability density function for the wave height did not change significantly, but for longer distances into the vegetation and higher incident waves it tended to be less similar to a Rayleigh distribution and more similar to the theoretically developed transformed distribution, where the higher waves are more damped than the smaller. Relationships developed in this study can be employed for management purposes to reduce resuspension and erosion in shallow lakes.

---

<sup>1</sup> Ph.D. Student, Water Resources Engineering, Lund University, Box 118, 221 00 Lund, Sweden. E-mail: charlotta.borell\_lovestedt@tvrl.lth.se

<sup>2</sup> Professor, Water Resources Engineering, Lund University, Box 118, 221 00 Lund, Sweden.

**Subject headings:** Vegetation; Wave attenuation; Wave spectra; Erosion; Lakes;  
Environmental Engineering

## **Introduction**

### *Background*

Wave energy dissipation in vegetation has several engineering and ecological applications. Waves at ocean shores are known to lose energy in kelp beds (Mendez and Losada 2004), seagrass meadows (Fonseca and Cahalan 1992), saltmarsh vegetation (Knutson et al. 1982; Möller and Spencer 2002; Möller 2006), and mangrove forests (Massel et al. 1999; Mazda et al. 2006; Quartel et al. 2007). These vegetated belts act as buffer zones protecting nearshore structures and ecosystems (e.g., Asano et al. 1992). In shallow lakes and wetlands, submerged and emergent vegetation are known to reduce resuspension of bottom sediments by decreasing the wave energy (Hamilton and Mitchell 1996; Horppila and Nurminen 2001; Houwing et al. 2002). This reduction has several ecological effects as light climate is enhanced and internal loading of sediment-bound nutrients is reduced.

The effect of submerged macrophytes on wave-induced resuspension in shallow lakes has been the subject of several investigations (e.g., Blindow et al. 2002; Houwing et al. 2002), whereas the impact from emergent vegetation is less known. One main advantage for emergent vegetation, like reed, is that it is not negatively affected by higher turbidity as is the submerged vegetation. A common problem in shallow lakes all over the world is the loss of submerged vegetation due to lower light availability as a consequence of increased nutrient loading and subsequent algal blooms (e.g., Scheffer et al. 1993; Hamilton and Mitchell 1997; Rasmussen and Anderson 2005). Left to protect the sediment from resuspension is the emergent vegetation, commonly growing along the shores of these ecosystems.

### *Previous studies*

Knowledge on the damping of waves in vegetation has been provided by theoretical models, laboratory experiments and to a limited extent by field measurements. Dalrymple et al. (1984) used linear wave theory to describe the wave energy dissipation in clusters of cylinders representing the effect of giant kelp or submerged trees in overland flooding during hurricane events. The same approach may be used for emergent reed vegetation as the geometry of the reed belt is similar to a cluster of cylinders. Kobayashi et al. (1993) further developed the model of Dalrymple et al. (1984) and showed that it predicted wave decay in submerged kelp vegetation in laboratory experiments with reasonable accuracy. They improved the model by including the swaying motion of the vegetation (Asano et al. 1992) and later combined the wave model with a current model (Ota et al. 2005). Mendez and Losada (2004) also used the model of Dalrymple et al. (1984) and added the effect of shoaling and wave breaking to analyze the transformation of waves over vegetated fields. The model described the wave transformation over artificial submerged kelp in the laboratory well. Dean and Bender (2006) used linear wave theory to show that wave damping over vegetated areas had a significant effect on the static wave setup, where the vegetation was represented by emergent cylinders. The attenuation of uni-directional flow within vegetation has been well documented (Mazda et al. 1997; Nepf 1999; Leonard and Reed 2002; Tanino and Nepf 2008).

Most field studies have focused on the spatial change of one representative wave height (for example the significant wave height), thus approximating the waves to a monochromatic wave field, comparable to many laboratory experiments. In contrast,

waves in nature usually follow a Rayleigh distribution. This property was included in the model by Mendez and Losada (2004), although they assumed that the Rayleigh distribution was not modified by the vegetation belt.

Field data on wave damping in vegetation are rare compared to laboratory data; however, the attenuation by saltmarsh vegetation in coastal regions has been investigated in several studies (Knutson 1982; Möller and Spencer 2002; Möller 2006), and some experiments have been carried out in mangrove forests (Massel et al. 1999; Mazda et al. 2006; Quartel et al. 2007), and over kelp belts (Løvås 2000). Möller and Spencer (2002) showed that the reduction in significant wave height,  $H_s$ , was largest over the first 10 m of saltmarsh vegetation ( $1\text{--}2\% \text{ m}^{-1}$  for waves with incident  $H_s$  around 30 cm, and water depth of 1–3 m). In a later study Möller (2006) showed that the reduction in significant wave height,  $H_s$ , over the first 10 m of saltmarsh was about  $1\% \text{ m}^{-1}$  (with large variability ranging from  $0.008$  to  $3\% \text{ m}^{-1}$ ) when incident  $H_s$  was about 20 cm and water depth was below 1 m. Fonseca and Cahalan (1992) showed that the wave heights over different types of seagrass were reduced by approximately 40% over 1.0 m of vegetation in the laboratory when the incident wave height was 2–4 cm.

Wave damping due to vegetation in lakes has been even less investigated than in the ocean, especially with regard to field measurements, although its indirect effects on the light climate are well known (e.g., Hamilton and Mitchell 1996). However, the damping of waves over submerged vegetation has been analyzed in the laboratory (Houwing et al. 2002). Also, the indirect effects have been studied by comparing turbidity in different lakes to the bottom coverage of submerged vegetation (Hamilton and Mitchell 1996). Thus, there is a need for further knowledge on the direct coupling

between turbidity, resuspension, and wave damping in vegetation in shallow lakes and wetlands.

The wave damping effects by common reed (*Phragmites australis*) has been investigated together with another emergent species (*Scripus lacustris*) in a tank experiment by Coops et al. (1996) to analyze the potential for erosion protection from ship-induced waves at river banks. They showed that *Phragmites australis* reduced the wave height most effectively and this reed was also most capable to withstand the wave energy, while *Scripus lacustris* was damaged.

Wave damping in vegetation depends on the geometrical (e.g., diameter, branching, height) and physical characteristics (e.g., flexibility, buoyancy) of the plant. Vegetation reaching the water surface and above is more effective in reducing wave height than deeply submerged vegetation (Kobayashi et al. 1993). Many investigations on wave damping in vegetation (e.g., Kobayashi et al. 1993; Massel et al. 1999; Quartel et al. 2007) aimed to find a drag coefficient to predict the wave energy dissipation for a specific type of geometry or plant species. This drag coefficient sometimes includes the geometry of the plant (Quartel et al. 2007), but preferably it should be independent of geometrical parameters enabling modeling of the same type of vegetation with varying geometries, for example spacing and stem diameter. Mendez and Losada (2004) related the drag coefficient to a Keulegan-Carpenter number and expressed the need for further investigation of the dependence on this number for different types of plants. To achieve a better understanding of the resuspension in lakes more laboratory and field data on damping due to vegetation are needed (Teeter et al. 2001), as well as on drag coefficients for different vegetation types (Kobayashi et al. 1993).

### *Objectives and procedure*

The damping of wind waves in reed vegetation in a shallow lake was studied to improve the understanding of emergent vegetation for the light climate and shore stabilization in such ecosystems. There is a lack of knowledge on energy dissipation and wave height distribution changes for natural waves in reed vegetation (*Phragmites australis*). Thus, this study aimed at (1) examining the damping effects to find a species-specific drag coefficient independent of the density and stem diameter of the vegetation, and (2) analyzing possible changes in the probability density function for waves traveling through the vegetation.

Field experiments were carried out to collect data on wave heights outside and within the vegetation in a shallow lake. Thereafter a mathematical model describing the wave height reduction within the vegetation was developed based on linear wave theory. A model for probability density function transformation due to vegetation was also derived using a wave-by-wave approach. Finally, the predictions by the models were compared with the field data.

### **Theoretical Developments**

#### *Transformation of monochromatic waves*

The transformation of the waves through a reed belt may be described by the wave energy flux conservation equation, which is written for non-breaking monochromatic, normally incident waves using linear wave theory,

$$\frac{d}{dx}(EC_g) = -D_r - D_f \quad (1)$$

where  $E$  = wave energy density ( $= 1/8 \rho g H^2$ ; see below);  $C_g$  = wave group speed ( $= n \cdot C$ ;  $n = (1+2kd/\sinh 2kd)/2$ ;  $C = \sigma/k$ ; see below);  $D_r$  = energy dissipation due to the reed belt;  $D_f$  = energy dissipation due to the bottom friction; and  $x$  = coordinate originating at the seaward end of the reed belt pointing onshore. The dissipation caused by the reed belt are expressed as (Dalrymple et al. 1984),

$$D_r = \frac{2}{3\pi} C_D \rho N D H^3 \left( \frac{gk}{2\sigma} \right)^3 \frac{\sinh kd (\cosh^2 kd + 2)}{3k \cosh^3 kd} \quad (2)$$

where  $C_D$  = depth-averaged drag coefficient;  $\rho$  = water density;  $N$  = reed density (number of vegetation stands per unit horizontal area);  $D$  = diameter of an individual reed stand;  $H$  = wave height;  $g$  = acceleration due to gravity;  $k$  = wave number;  $\sigma$  = wave frequency; and  $d$  = water depth. Eq. (2) is derived by integrating the total force over the water depth and averaging over a wave period, expressing the force on the reed at any particular time and depth by a Morison-type equation (Chakrabarti 1987). The energy dissipation due to bottom friction is given by (Nielsen 1992),

$$D_f = \frac{2}{3\pi} \rho f_D U_b^3 \quad (3)$$

where  $f_D$  = wave energy dissipation coefficient; and  $U_b$  = horizontal bottom orbital velocity amplitude. From linear wave theory, the velocity  $U_b$  is obtained as:

$$U_b = \left( \frac{gk}{2\sigma} \right)^3 \frac{1}{\cosh^3 kd} H^3 \quad (4)$$

Thus, both  $D_r$  and  $D_f$  depend on  $H^3$  as well as on some function of the water depth (or  $x$ , if the relationship between  $h$  and  $x$  is known).

Substituting in Eqs. (2) and (3) into Eq. (1) yields:

$$\frac{d}{dx}(EC_g) = -\frac{2}{3\pi}\rho\left(\frac{gk}{2\sigma}\right)^3 \frac{1}{\cosh^3 kd} \left( C_D ND \frac{\sinh kd (\cosh^2 kd + 2)}{3k} + f_D \right) H^3 \quad (5)$$

In order to allow for a closed-form solution in the general case, the wave energy flux  $F = EC_g$  is introduced in Eq. (5) together with the two functions,  $\psi_1$  and  $\psi_2$ , which both depend on the water depth (or  $x$ ),

$$\frac{d}{dx}(F) = -\psi_1 (C_D \psi_2 + f_D) F^{3/2} \quad (6)$$

where:

$$\psi_1 = \frac{2}{3\pi} \left( \frac{gk}{2\sigma} \right)^3 \frac{1}{\cosh^3 kd} \frac{8^{3/2}}{\sqrt{\rho} g^{3/2} C_g^{3/2}} \quad (7)$$

$$\psi_2 = ND \frac{\sinh kd (\cosh^2 kd + 2)}{3k} \quad (8)$$

The solution to Eq. (6) is,

$$F = \left( \frac{1}{\sqrt{F_o}} + \frac{1}{2} \int_0^x \psi_1 (C_D \psi_2 + f_D) dx \right)^{-2} \quad (9)$$

where  $F_o$  is the wave energy flux at  $x=0$ . For the case of a constant water depth, Eq. (9) simplifies to:

$$F = \frac{F_o}{\left( 1 + \frac{1}{2} \sqrt{F_o} \psi_1 (C_D \psi_2 + f_D) x \right)^2} \quad (10)$$

Eq. (10) may be expressed in terms of the wave height,

$$H = \frac{H_o}{1 + \frac{1}{2} \sqrt{F_o} \psi_1 (C_D \psi_2 + f_D) x} \quad (11)$$

where  $H_o$  is the wave height just outside the reed belt. If bottom friction is negligible, Eq. (10) can be further reduced to:

$$H = \frac{H_o}{1 + \frac{1}{2} \sqrt{F_o} \Psi_1 C_D \Psi_2 x} \quad (12)$$

Eq. (12) is identical to the solution presented by Mendez and Losada (2004), who studied propagation of random waves over vegetation fields.

#### *Transformation of probability density function*

Eqs. (9) to (12) were derived for monochromatic waves, and such equations are often employed to field conditions using a representative wave height (e.g., the root-mean-square (rms) or significant wave height). In the field, however, waves are random in their character with varying height, period, and direction. The assumption is often made that the wave field is narrow-banded in period and direction and the randomness enters primarily through the wave height (Dally 1990; Larson 1995), and this assumption will also be made here. Mainly two approaches exist to model the transformation of random waves: (1) making an assumption about the general form of the probability density function (pdf) and integrating the governing equation using the assumed pdf to arrive at a wave transformation equation valid for random waves (Battjes and Janssen 1978, Thornton and Guza 1983); and (2) using a wave-by-wave approach where the pdf in the offshore is assumed and individual waves in this pdf are transformed onshore after which they are superimposed to obtain the local pdf across the domain (Dally 1990, Larson 1995). Here the latter approach will be employed to derive the wave height pdf at

any location  $x$  in the reed belt. Mendez and Losada (2004) took the former approach when they developed their random wave transformation model.

It is assumed that the wave height outside the reed belt are described by a Rayleigh pdf according to,

$$p(H_o) = \frac{2H_o}{H_{rmso}^2} \exp\left(-\left(\frac{H_o}{H_{rmso}}\right)^2\right) \quad (13)$$

where  $H_{rmso}$  is the root-mean-square wave height, and subscript  $o$  denotes the location outside the reed belt. Every individual wave making up the pdf outside the reed belt is described by Eq. (12) as it propagates through the reed. The transformation of the pdf is given by,

$$p(H) = p(H_o) \left| \frac{dH_o}{dH} \right| \quad (14)$$

where  $p(H)$  is the pdf for the transformed wave height. Expressing  $H_o$  as a function of  $H$  using Eq. (12) yields (note that  $F_o = 1/8\rho g H_o^2 C_g$ ),

$$H_o = \frac{H}{1 - \frac{1}{2}xBH} \quad (15)$$

where the coefficient  $B$  was introduced:

$$B = \left(\frac{1}{8}\rho g C_g\right)^{1/2} \Psi_1 \Psi_2 C_D \quad (16)$$

Taking the derivative of  $H_o$  with respect to  $H$  in Eq. (15) and substituting it into Eq. (14) together with Eq. (13) yields:

$$p(H) = \frac{2}{H_{rmso}^2} \frac{H}{\left(1 - \frac{1}{2}xBH\right)^3} \exp\left(-\left(\frac{1}{H_{rmso}} \frac{H}{1 - \frac{1}{2}xBH}\right)^2\right) \quad (17)$$

Although the Rayleigh pdf has no upper limit on the wave height, Eq. (15) is only meaningful if  $xBH < 2$ , implying an upper limit for the wave height in the pdf given by Eq. (17) according to  $H < 2/xB$ . If  $x \rightarrow 0$ , Eq. (17) reverts to Eq. (13) with the upper limit  $H_o \rightarrow \infty$ .

Fig. 1 illustrates the transformed pdf given by Eq. 17 in non-dimensional form for different values of the parameter  $xBH_{rmso}$ . Since the dissipation is proportional to  $H^3$ , the larger waves experience more dissipation than the smaller waves, and the pdf changes shape with more probability mass being concentrated to lower wave heights. The further away the waves propagate from the starting point outside the reed belt, the larger the dissipation is and the more the pdf becomes skewed towards lower wave heights.

## Field Measurements

### *Field site*

Wave damping in reed vegetation was measured during July 2006 in the shallow Lake Krankesjön (55°42'N, 13°28'E) in southern Sweden. The lake is classified as a Wetland of International Importance according to the Ramsar Convention on Wetlands, and it is also included in the Natura 2000 ecological network, established by the European Union to protect rare and endangered species and habitats. The surface area is 3 km<sup>2</sup> and the maximum and mean depths are 3.0 and 0.7 m, respectively. Wind-induced resuspension of bottom sediments has been found to be the main mechanism affecting the

light availability in the lake (Blindow et al. 2002). Lake Krankesjön is moderately eutrophic and has a rich cover of reeds, mainly *Phragmites australis*, along the entire shoreline. The growing season of reed is from the beginning of May until the end of September. Two sites with different density of vegetation and different depths were chosen for the field measurements; the shallow site and the deep site (Fig. 2). It should be noted that the names refer to the absolute depth at the site and that the relative depth concerning wave theory were deep or transitional (close to deep) at both sites.

Average stem diameter and number of stands per unit area were measured at the two sites. The stem diameter was measured at the still water level around the transect and the number of stands was measured using a  $0.5 \times 0.5$  m frame. All measurements were made from a small boat except for the vegetation density at the shallow site, where wading was possible, thus minimizing disturbance of the reed vegetation. Maps of the vegetation density were drawn for each site (Fig. 3) from a large number of measurements (40 at the shallow site and 20 at the deep site) within and around the transect, ensuring a good characterization of the reed density. As natural growing reed is highly variable, there is a random variation in stem diameter and density. Thus, the maps should be treated as schematic sketches with an approximate error of 25%. The transition between the open water and the vegetation was fairly sharp at the two measurement sites. Six poles, on which the wave gages were mounted during the measurements, were driven down into the bottom following an array at both sites. The depth was measured at each pole together with its location in a local coordinate system (Table 1).

At the shallow site the average depth at the poles was 0.41 m. One pole was placed immediately outside the vegetation as a reference for the incoming waves (Pole 1); the

others were placed in a line where the innermost pole was 5 m from the edge of the vegetation (Fig. 3; Table 1). The reed vegetation at the shallow site was a monoculture of *Phragmites australis* and the average stem diameter was 4.1 mm (standard deviation 1.0 mm, 24 samples). Uprooted macrophytes were found within the vegetation at this site, and these were removed before the measurements to not affect the waves.

The average depth at the deep site was 1.3 m and the two outermost poles (1 and 2) were placed outside the vegetation, pole 3 was at the boundary between the open water and the vegetation, and the innermost pole (6) was almost 4.5 m from the open water. The transect at the deep site was placed **next to** an area of lower density of vegetation so that the disturbance on the vegetation from the boat was minimized. However, it is possible that the boat had some effect on the density, i.e., breaking of individual stalks, although the remainders of the stalks below the water surface could still affect the waves. Overall, vegetation density was slightly higher at the deep site and the stems were thicker with an average diameter of 8.4 mm (standard deviation 1.4 mm, 9 samples). The vegetation was a monoculture of *Phragmites australis* (Fig. 2b).

#### *Field experiment techniques*

Two magnetostrictive displacement transducers (Santest Co.) were used as wave gages. These consisted of a metal rod (80 cm) with a float, surrounding the rod, which could easily move up and down along the rod. An electric signal that was linearly correlated to the position of the float on the rod, corresponding to the elevation of the water surface (error  $\approx 1$  mm), was sent from the wave gages to a data logger. The float responded immediately to surface level changes (waves) and was only observed to miss

the top of waves for a few of the highest waves (cutting of approximately 0.5 cm). Whenever this was observed it was noted as float overtopping. The advantage of this technique in relation to the common method of pressure transducers is that the surface elevation is measured directly, without the need to correct for the pressure induced by the wave dynamics. The technique resembles the “Swartz poles” used by Young and Verhagen (1996) to measure waves in a shallow lake. The logger recorded the surface elevation at 8–10 Hz, which means that waves with short periods, below 1 s, corresponding to wave heights down to a few millimeters, were recorded. The wave gages were always mounted at the side of the pole heading the incident waves so that the poles did not affect the measured waves, and the float was always free to move without any interference from the vegetation or floating debris.

Wave measurements were performed on three occasions at the shallow site and on five occasions at the deep site. As there were only two wave gages available, one was always mounted at the outermost pole (Pole 1), while the other wave gage was moved between Poles 2–6. At each pole the surface elevation was measured for 3 minutes, after which the wave gage was moved to the next pole during a 7 minute break between each measurement. At every occasion, waves were first measured at Pole 1 and 2, then the wave gage was moved from Pole 2 to Pole 3, from Pole 3 to Pole 4, and so on until Pole 6 was encountered. Thereafter the same procedure was performed again but starting with Pole 1 and Pole 6 and then moving the wave gage from Pole 6 and seawards to Pole 2. This will be referred to as one measurement cycle.

During each measurement cycle the wind speed was measured several times with a hand held wind gage (Silva Windwatch) and wind direction was noted using a compass.

The incident angle of the waves was estimated using a protractor as it was not parallel to the transect spanning the poles (approximate error = 10°). Based on the incident wave angle, the distance for the waves to travel from the edge of the reed belt to the wave gage was calculated ( $x$ ). The reed density ( $N$ ), was estimated from the maps for each  $x$ . Wave breaking was not observed during any of the wave measurements.

The surface level data from the recordings were translated into wave parameters using the zero-down crossing method. Linear wave theory was assumed to be valid, and the wave height time series for each three-minute recording was used to determine the root-mean-square wave height;

$$H_{rms} = \sqrt{\frac{1}{m} \sum_{i=1}^m H_i^2} \quad (18)$$

where  $m$  = the number of recorded waves; and  $H$  = the height of each individual wave. Individual wave heights were used to analyze the pdf transformation. The full equations for transitional water depth was used for the wave theory (i.e., the simplifications for shallow or deep water was not used), although deep-water conditions prevailed in almost all cases.

The development of wind waves in Lake Krankesjön has been shown to be similar to wind waves in the open ocean (Fig. 4), showing good correlation with the predicted wave heights using fetch-limited deepwater wave forecasting equations (U.S. Army Coastal Eng. 1984). The waves and wind were measured in the open water in Lake Krankesjön in 2006 using the same technique as described above. The significant wave height ( $H_s$ ) was determined as the average height of the 1/3 highest waves. This implies that the predictive equations developed for wind waves in the ocean are useful also for shallow lake waves.

## Results – Measurements and comparison with modeling

### *Field measurements*

Average incident root-mean-square wave heights ranged between 5 and 6 cm at the shallow site (Table 2) and 1 to 5 cm at the deep site (Table 3) for each cycle, which represents medium wave heights for Lake Krankesjön. Maximum  $H_{rms}$  during all 3-minute periods was 8 cm. The average wave period at the shallow site was 1.0 s (range: 0.9–1.2 s) and 0.8 s (range: 0.5–1.0 s) at the deep site. Wind speeds were generally higher during the measurements at the shallow site (6–10 m s<sup>-1</sup>) than at the deep site (1.5–6 m s<sup>-1</sup>), which explains the higher waves at the shallow site. All measurement cycles showed decreasing wave heights with distance traveled within vegetation (Fig. 5 and 6). The average decrease was approximately 5% m<sup>-1</sup> at the shallow site and 4% m<sup>-1</sup> at the deep site over the first 5–14 m of reed vegetation.

### *Wave height decay and drag coefficient for reed*

A species-specific drag coefficient,  $C_D$  was determined by fitting Eq. 12 to the observed wave heights using three different approaches estimating: 1) an individual value of  $C_D$  for each 3-minute measurement period, resulting in perfect match between calculated  $H_{rms}$  and measured  $H_{rms}$ , 2) one value of  $C_D$  for each of the two sites giving the smallest root-mean-square-error, rmse (Eq. 18 with  $H_i$  replaced by  $H_{rms} (calculated)_i - H_{rms} (measured)_i$ , and  $m$  replaced by number of  $H_{rms}$ ), hereafter called the site specific  $C_D$ , and 3) one single value of  $C_D$  giving the smallest rmse for all data.

The individual  $C_D$  for each 3-minute period ranged between 0 and 80 (average 25; the range 5–35 included 74% of the values) for the shallow site, whereas corresponding values for the deep site was 0–164 (average 15; the range 4–25 included 90% of the values).

The best fit value using approach 2 (Fig. 7a) was 16.4 (rmse=0.0030 m) for the shallow site and 6.7 (rmse=0.0025 m) for the deep site, whereas the overall best fit was 9.0 (approach 3; Fig 7b; rmse=0.0039 m). For both sites together, 81% of the values of  $C_D$  were within 3–25.

#### *Transformation of probability density function*

As described earlier, higher waves should in theory be more damped than lower waves, which means that the probability density function (pdf) of the wave heights would change from the incident Rayleigh distribution to the transformed distribution as the waves propagate through the vegetation (Eq. 17, Fig. 1). Therefore, the pdf of the waves for each 3-minute measurement period was analyzed and compared to the incident pdf and evaluated with respect to the distance traveled in the vegetation.

Selected representative histograms and theoretical pdfs are shown in Fig. 8. When comparing only the histograms it is clear that when the waves traveled through the vegetation (Pole 4–6), the largest waves decayed and the peak of the histogram was shifting towards smaller waves. Different theoretical distribution curves were compared to the histograms: a Rayleigh distribution depending on the measured  $H_{rms0}$  and the transformed distribution curve for the waves within the vegetation (Eq. 17; site specific  $C_D$ ) compared with a Rayleigh distribution depending on the calculated  $H_{rms}$  (using Eq.

12, Eq. 13 (but with  $H$  instead of  $H_o$ ), and the site specific  $C_D$ ). The pdf for the incident waves at both sites were close to the Rayleigh distribution. Overall, the distribution in the vegetation at the shallow site was better described by the transformed pdf, while for the deep site the Rayleigh pdf was slightly better (Fig. 8). The rmse between the theoretical distributions and the measured histograms within the vegetation was analyzed for all three-minute periods. This showed that the modified distribution was better than the Rayleigh distribution at the shallow site during 67% of the measurement periods, while the Rayleigh distribution produced a smaller error for 22% of the periods (and there was no difference between the distributions for 11% of the periods). For the deep site the situation was the opposite: during 70% of the periods the Rayleigh distribution was better, while the modified distribution was better for 27% of the periods. The transformed function described the distribution better for 83% of the distributions for the 10% highest  $H_{rmso}$ , compared to 0% for the 10% lowest  $H_{rmso}$ .

An important question was whether the shape of the distribution changed significantly due to the drag in the vegetation. Thus, pdfs for both incident waves outside the vegetation and waves within the vegetation for all measurement periods were made non-dimensional and compared (Fig. 9). The comparison revealed that the difference between the mean distribution for the incident waves and the waves within the vegetation at both sites was small and within the standard deviation of the data from both sites. For the higher waves ( $H_{rmso} > 3$  cm) that had traveled a significant distance within the vegetation ( $x > 3$  m) a tendency can be seen in Fig. 9d for the pdf in the vegetation to be shifted towards the transformed pdf, with a narrower spectrum consisting of a smaller number of high waves and a larger number of medium waves, and with the peak shifted

towards smaller waves. However, this shift in the spectrum was within the standard deviation.

## **Discussion**

### *Field measurements*

Incident wave heights during the measurements were 5–6 cm at the shallow site and 1–5 cm at the deep site, which are medium wave heights for lakes of the depth and size of Lake Krankesjön. The wave gages were easy to use, and the obtained data were directly transferred to wave parameters. However, as natural lake waves are characterized by great variability, both in space and time, and the waves in the experiment were small, the data include a degree of variation and measurement uncertainty. It is not possible to separate the natural variation from the measurement uncertainty, but the result of these can be seen, for example, in Fig. 5 and 6, where there are values of  $H_{rms}/H_{rms0} > 1$ . Since pole 3 was at the boundary between the open water and the vegetation at the deep site there are also  $H_{rms}/H_{rms0}$ -values at  $x=0$ , referring to the difference between pole 1 and 3 (no wave damping). The spatial variation has a greater effect if the incident angle deviation from the direction of the transect is larger. Measurement errors in the incident angle also produces greater errors in  $x$  as the angle increases. A comparison between the wave height at pole 1 and at pole 2–3 at the deep site, gave a measure of the uncertainty of the wave measurements as both poles 2 and 3 were outside the vegetation. The overall root-mean-square-error was 0.2 cm, but depending on incident wave height. The mean error for  $H_{rms0} < 2$  cm was 10%, whereas it was 5% for  $H_{rms0} > 2$  cm. Smaller waves are presumably associated with greater errors as the measurement speed (8–10 Hz) limits the

detection and accuracy of waves with very short wave periods. At the deep site, the incident angle was larger and the waves were smaller and more varying than at the shallow site, which is probably the reason for the greater scatter in the data from this site. The lowest waves ( $H_{rms0} < 2$  cm) are indicated with the grey-filled symbols in Fig. 6, illustrating the greater variation for these waves.

The average attenuation of the waves within the first 5–14 m of reed vegetation was approximately  $5\% \text{ m}^{-1}$  at the shallow site and  $4\% \text{ m}^{-1}$  at the deep site, which is comparable to  $1\text{--}2\% \text{ m}^{-1}$  that was found over the first 10 m in a coastal saltmarsh, where  $H_s$  of the incident waves was about 30 cm (Möller and Spencer 2001). Möller and Spencer also showed that the attenuation (in percentage per meter) was greatest over the first 10 m of vegetation. Knutson et al. (1982) also found that the damping in a saltmarsh decreased with the distance traveled through vegetation ( $16\% \text{ m}^{-1}$  over the first 2.5 m and  $3\% \text{ m}^{-1}$  averaged over 30 m). The damping in vegetation is thus not linear, and also depend on the incident wave characteristics (Eq. 2), which is accounted for in the model used in this study (Eq. 12).

#### *Drag coefficient for reed*

The drag coefficient for the shallow site using approach 2 was 16.4, with an interval of most probable values from 5–35, whereas the corresponding value was 6.7 (4–25) for the deep site. The overall best fit value of  $C_D$  (approach 3) was found to be 9, and the most probable interval was 3–25. The obtained drag coefficient values can be compared to  $C_D$ -values for natural mangrove vegetation of 0.4–10 (Mazda et al. 2006), and for artificial kelp in a wave tank of 0.1–12 (Kobayashi et al. 1993). It is important when

comparing different studies on  $C_D$  to note whether monochromatic waves,  $H_{rms}$ , or  $H_s$  is used in the models and also if the drag coefficient includes the geometry of the vegetation. Values found in the literature on  $C_D$  for steady flow passing an infinite circular cylinder are around 1 for Reynolds numbers within the range of this study (e.g., Franzini and Finnemore 1997).

The prediction of  $H_{rms}$  (Eq. 12) using the two site specific  $C_D$ -values (Fig. 7a), or using one  $C_D$ -value for both sites (Fig. 7b) yield good agreement with the measured  $H_{rms}$  (rmse for the site specific values was 0.3 cm for the shallow sites and 0.25 cm for the deep site, whereas rmse was 0.39 cm for the third approach).

The higher value of  $C_D$  obtained at the shallow site is most likely due to the presence of subsurface old roots and straws, as well as some floating debris (although as much as possible was cleaned away) affecting the drag coefficient. There could also have been some impact from the bottom as the ratio  $d/L$ , where  $L$  is the wavelength, indicated that the depth was transitional, although it was close to deep water waves (defined as  $d/L > 0.5$ ). The relative depth at the deep site was always above 0.5.

Many studies have obtained a relationship between  $C_D$  and Reynolds number,  $Re$ , (Kobayashi et al. 1993; Mazda et al. 2006) or a Keulegan-Carpenter number,  $K$ , (Mendez and Losada 2004), where  $C_D$  decreases with  $Re$  or  $K$ . The data collected in this study (from approach 1) do not indicate a clear correlation between  $C_D$  and any of these numbers (Fig. 10), where  $Re$  was defined as,

$$Re = \frac{u_{max} \cdot D}{\nu} \quad (19)$$

where  $u_{max}$  = maximum horizontal water particle velocity at the water surface ( $\text{m s}^{-1}$ ; estimated from wave theory), and  $\nu$  = kinematic viscosity of water ( $1.005 \times 10^{-6} \text{ m}^2 \text{ s}^{-1}$  at  $20^\circ\text{C}$ ), and a modified Keulegan-Carpenter number,  $K'$  was calculated from:

$$K' = \frac{u_{max} \cdot T}{D} \quad (20)$$

Kobayashi et al. (1993), found a negative correlation between  $C_D$  and Re for  $2200 < \text{Re} < 18000$ , and Mazda et al. (2006) also found a negative correlation between  $C_D$  and Re for  $10^4 < \text{Re} < 5 \times 10^4$ . The range of Re in the present study was 90–1320, but it should be noted that the definition of Re is not the same in the different studies. The uncertainty in the estimated  $C_D$ -values (see below) together with the relatively small range of Re-values can be one reason why little correlation between these parameters was found in this study. However, the reason that the site specific  $C_D$  was higher at the shallow site could perhaps be explained by the overall lower Reynolds numbers at this site, and vice versa for the deep site. The Keulegan-Carpenter number used by Mendez and Losada (2004), was calculated from Eq. 20 but with the depth-averaged maximum particle velocity,  $u_c$ , which is only useful for shallow and transitional depths, instead of  $u_{max}$ . They found a negative correlation between  $C_D$  and  $K$  for  $K < 60$  and  $C_D < 0.55$ . In this study  $K'$  is not a suitable parameter to compare with  $C_D$  since the data from the two sites form two separate groups (Fig. 10b).

In Fig. 10 all the high values of  $C_D$  ( $>30$ ) for the shallow site can be identified as drag coefficients calculated for small  $x$ -values ( $<2.3 \text{ m}$ ). These higher values are probably related to a greater uncertainty in  $N$  and  $D$  for short distances from the open water, since the natural randomness of the vegetation tend to approach the estimated average values after longer distances. The drag coefficient dependence on  $x$  can be seen in Fig. 11, most

clearly for the shallow site (Fig. 11a). The scatter in  $C_D$ -values at the deep site was also greater for smaller wave heights (<2 cm).

The uncertainty in the measured  $D$ ,  $N$ , and the incident angle of the waves also affects the estimated drag coefficients. A 25% error in the measured  $N$  gives an error of approximately 25% in  $C_D$  for average  $N$ -values (greater effect on  $C_D$  for smaller  $N$ -values). For the stem diameter, a 25 % error around the average  $D$  results in approximately 20% error in  $C_D$  (greater effect on  $C_D$  for smaller  $D$ -values). Errors in the incident angle also affect the obtained  $C_D$ -values (see above). Furthermore, there is a greater uncertainty in  $N$  and  $D$  for larger incident wave angles since most of the measurements of these parameters were made close to the transects. Also,  $C_D$  is a depth-averaged value and the geometry of the vegetation is measured at the surface, where the drag will be the highest since the orbital velocities is the highest. The vegetation characteristics may vary with depth, possibly by an increase in diameter and a higher density due to stems not reaching the surface, which will affect the drag.

The calculated wave height decays for different  $C_D$ -values, with all other parameters held constant (chosen as the average values of all measurements at both sites), is presented in Fig. 12, showing that the difference in decay for a relatively large range of  $C_D$ -values is comparable to the variation in the field data (Fig. 5 and 6). However, the field data also include the variation in incoming wave parameters. Despite the uncertainty in the field measurements and the natural variation in both waves and vegetation, it has been shown that using an average value of  $C_D=9$ , the wave height decay in reed vegetation can be predicted with an accuracy of 0.39 cm (rmse) for varying diameter and density of the vegetation within the range of wave parameters studied (Fig. 7).

### *Transformation of probability density function*

The results of the pdf analysis indicated that the distribution is relatively unchanged if the waves are damped by the vegetation, implying that the assumption made by Mendez and Losada (2004) that the pdf does not change is reasonable, at least in an average sense. The pdfs within the vegetation at the shallow site, however, tended to follow the transformed pdf (Fig. 8), which probably is a result of the higher incident waves being more affected by the vegetation. For some periods at the deep site,  $xBH$  was close to the upper limit for Eq. 17 to be valid ( $xBH < 2$ ) which could also explain why this pdf did not yield as good agreement as the Rayleigh distribution. Furthermore, there was a tendency that the distributions for higher  $H_{rms0}$  and larger  $x$  deviated from the incident distribution (Fig. 9d), although within a standard deviation. This standard deviation was relatively large which can be related to the variability in wave heights with time, but also that the measurement periods (3 minutes) could have been too short to establish an accurate pdf. More data on distributions including higher waves is needed to provide reliable conclusions.

### **Conclusions**

The wave measurements in this study showed that there was a significant damping of wave heights due to drag against reed vegetation (average value of 4–5%  $m^{-1}$  over the first 4–15 m for  $H_{rms0}$  of 1–6 cm). The analysis of the wave height decay showed that  $C_D$  for reed vegetation (*Phragmites australis*), can be approximated to 9 (most probable range: 3–25) for  $H_{rms0}$  within the range of the wave heights studied. There was a

significant variation in  $C_D$  between the single 3-minute measurement periods. However, since the wave heights within the vegetation was well predicted using Eq. 12, with an average drag coefficient for both sites (Fig. 7),  $C_D = 9$  could probably be used for management purposes with a reasonable accuracy. Since  $C_D$  did not show any correlation with  $Re$  for the data investigated, this coefficient can be taken as a constant for similar conditions.

The applicability of the transformation of the wave height probability distribution within the vegetation derived in this study was not conclusively proven, even though it can not be excluded as the waves were relatively small. The data from measurement periods with higher  $H_{rms0}$  tended to show a greater similarity with the transformed distribution than with the Rayleigh distribution.

This study quantitatively identified the damping of waves in reed vegetation, and relationships were developed that can be used for management purposes to stabilize shores and nearshore bottoms of shallow lakes and wetlands. The reduction in resuspension in nearshore areas of lakes by emergent vegetation can for example be determined using Eq. 12, linear wave theory, and knowing the critical bottom conditions for suspension. The minimum vegetation cover needed for shore/near-shore bottom stabilization can thus be calculated. The wave decay model could probably also be used for other types of water bodies where waves and vegetation of similar properties as in this study occur.

Since the measured waves were rather small, their erosional effect may be questioned. However, the maximum wave height observed in the studied lake is not considerably higher (around  $H_{rms}=15$  cm; Fig. 4;  $H_s > H_{rms}$ ) and the resuspension of bottom

sediments due to waves is well documented in Lake Krankesjön (e.g., Blindow et al. 2002). From aerial photographs it is clear that the shores located at the few openings in the reed vegetation are eroding. This further proves the importance of nearshore emergent vegetation for shore protection in such ecosystems.

The wave measurement method was applicable and the only limitations are that the gages have to be mounted on a pole and that the length of the rod (in this case 80 cm) limits the upper wave heights that can be measured, whereas the speed of the data logging sets the lower wavelength (and thereby indirectly wave height) limitation. For the highest and steepest waves, the top was sometimes missed (about 0.5 cm). More data could have been generated if one logger was mounted simultaneously on each pole. The method used in this study, where one gage was always measuring the incident wave heights, assured that the variation in  $H_{rms}$  with time was recorded so that the  $H_{rms}$  and  $H_{rms0}$  compared were always measured at the same time.

### **Acknowledgements**

We would like to thank Per Falås for the help with field measurements and Revinge Bysamfällighet for providing us with boats. Kungliga Fysiografiska Sällskapet and Åke och Greta Lissheds Stiftelse contributed financially to the field equipment. [We are also thankful for the comments from three anonymous reviewers, which significantly improved the report.](#)

### **Notation**

$B$  = coefficient

$C_D$  = depth-averaged drag coefficient

$C_g$  = wave group speed

$C$  = wave speed

$d$  = water depth

$D$  = diameter of an individual reed stand

$D_f$  = energy dissipation due to bottom friction

$D_r$  = energy dissipation due to reed belt

$E$  = wave energy density

$f_D$  = wave energy dissipation coefficient

$F$  = wave energy flux

$g$  = acceleration due to gravity

$H$  = wave height

$H_{rms}$  = root-mean-square wave height

$H_s$  = significant wave height

$k$  = wave number

$K$  = Keulegan-Carpenter number

$K'$  = modified Keulegan-Carpenter number

$L$  = wavelength

$N$  = reed density (number of vegetation stands per unit horizontal area)

$m$  = number of waves

$p$  = probability

rmse = root-mean-square-error

Re = Reynolds number

$u_c$  = depth-averaged maximum particle velocity

$u_{max}$  = maximum horizontal water particle velocity at the water surface

$U_b$  = horizontal bottom orbital velocity amplitude

$x$  = coordinate originating at the seaward end of the reed belt pointing onshore

$\nu$  = kinematic viscosity

$\rho$  = water density

$\sigma$  = wave frequency

$\psi_1, \psi_2$  = functions

### **Subscripts**

$o$  = the location just outside the reed belt

## References

- Asano, T., Deguchi, H. and Kobayashi, N. (1992). "Interaction between water waves and vegetation." *Proc., 23<sup>rd</sup> Coastal Eng. Conf.*, ASCE. 2710–2723.
- Battjes, J.A. and Janssen, J.P.F.M. (1978). "Energy loss and setup due to breaking of random waves." *Proc., 16<sup>th</sup> Coastal Eng. Conf.*, ASCE. 569–587.
- Blindow, I., Hargeby, A. and Andersson, G. (2002). "Seasonal changes of mechanisms maintaining clear water in a shallow lake with abundant *Chara* vegetation." *Aquat. Bot.*, 72, 315–334.
- Chakrabarti, S.K. (1987). "Hydrodynamics of offshore structures." Computational Mechanics Publications/Springer-Verlag.
- Coops, H., Geilen, N., Verheij, H.J., Boeters, R. and Velde, G.v.d. (1996). "Interactions between waves, bank erosion and emergent vegetation: an experimental study in a wave tank." *Aquat. Bot.*, 53, 187–198.
- Dalrymple, R.A., Kirby, J.T., and Hwang, P.A. (1984). "Wave diffraction due to areas of energy dissipation." *J. Waterway, Port, Coastal, Ocean Eng.*, 110(1), 67–79.
- Dally, W.R. (1990). "Random breaking waves: A closed-form solution for planar beaches." *Coast. Eng.*, 14, 233–263.
- Dean, R.G. and Bender, C.J. (2006). "Static wave setup with emphasis on damping effects by vegetation and bottom friction." *Coast. Eng.*, 53, 149–156.
- Fonseca, M.S. and Cahalan, J.A. (1992). "A preliminary evaluation of wave attenuation by four species of seagrass." *Est. Coast. Shelf Sci.*, 35, 565–576.
- Franzini, J.B. and Finnemore, E.J. (1997). "Fluid Mechanics." *McGraw-Hill*.

- Hamilton, D.P. and Mitchell, S.F. (1996). "An empirical model for sediment resuspension in shallow lakes." *Hydrobiologia*, 317, 209–220.
- Hamilton, D.P. and Mitchell, S.F. (1997). "Wave-induced shear stresses, plant nutrients and chlorophyll in seven shallow lakes." *Freshw. Biol.*, 38: 159–168.
- Horppila, J. and Nurminen, L. (2001). "The effect of an emergent macrophyte (*Typha angustifolia*) on sediment resuspension in a shallow north temperate lake." *Freshw. Biol.*, 46, 1447–1455.
- Houwing, E.J., Tánčzos, I.C., Kroon, A. and de Vries, M.B. (2002). "Interaction of submerged vegetation, hydrodynamics and turbidity; analysis of field and laboratory studies." *Proc. Marine Sci.*, 5, 441–453.
- Knutson, P.L., Bronchu, R.A. and Seelig, W.N. (1982). "Wave damping in *Spartina alterniflora* marshes." *Wetlands*, 2(1), 87–104.
- Kobayashi, N., Raichle, A.W. and Asano, T. (1993). "Wave attenuation by vegetation." *J. Waterway, Port, Coastal, Ocean Eng.*, 119(1), 30–48.
- Leonard, L.A. and Reed, D.J. (2002). "Hydrodynamics and sediment transport through tidal marsh canopies." *J. Coast. Res.*, SI 36, 459–469.
- Larson, M. (1995). "Model for decay of random waves in surf zone." *J. Waterway, Port, Coastal, Ocean Eng.*, 121(1), 1–12.
- Løvås, S.M. (2000). "Hydro-Physical Conditions in Kelp Forests and the Effect on Wave Damping and Dune Erosion." Doctoral Thesis, The Norwegian University of Science and Technology, Trondheim.
- Massel, S.R., Furukawa, K. and Brinkman, R.M. (1999). "Surface wave propagation in mangrove forests." *Fluid Dyn. Res.*, 24, 219–249.

- Mazda, Y., Wolanski, E., King, B., Sase, A., Ohtsuka, D. and Michimasa, M. (1997). "Drag force due to vegetation in mangrove swamps." *Mangroves and Salt Marshes*, 1: 193–199.
- Mazda, Y., Magi, M., Ikeda, Y., Kurokawa, T. and Asano, T. (2006) "Wave reduction in a mangrove forest dominated by *Sonneratia* sp." *Wetlands Ecology and Management*, 14, 365–378.
- Mendez, F.J. and Losada, I.J. (2004). "An empirical model to estimate the propagation of random breaking and nonbreaking waves over vegetation fields." *Coast. Eng.*, 51, 103–118.
- Möller, I. (2006). "Quantifying saltmarsh vegetation and its effect on wave height dissipation: Results from a UK East coast saltmarsh." *Est. Coast. Shelf Sci.*, 69, 337–351.
- Möller, I. and Spencer, T. (2002). "Wave dissipation over macro-tidal saltmarshes: Effects of marsh edge typology and vegetation change." *J. Coast. Res.*, SI 36, 506–521.
- Nepf, H.M. (1999). "Drag, turbulence, and diffusion in flow through emergent vegetation." *Water Resources Research*, 35, 479–489.
- Nielsen, P. (1992). "Coastal bottom boundary layers and sediment transport." *Advanced series on ocean engineering*, World Scientific, Singapore
- Ota, T., Kobayashi, N. and Kirby, J.T. (2005). "Wave and current interactions with vegetation." *Proc. 29<sup>th</sup> Int. Conf. Coastal Engineering, 2004*, ASCE, New York, 508–520.
- Quartel, S., Kroon, A., Augustinus, P.G.E.F., Van Santen, P. and Tri, N.H. (2007). "Wave attenuation in coastal mangroves in the Red River Delta, Vietnam." *J. Asian Earth Sci.*, 29, 576–584.

- Rasmussen, P. and Anderson, N.J. (2005). "Natural and anthropogenic forcing of aquatic macrophyte development in a shallow Danish lake during the last 7000 years." *J. Biogeogr.*, 32: 1993–2005.
- Scheffer, M., Hosper, S.H., Meijer, M.-L., Moss, B. and Jeppesen, E. (1993). "Alternative equilibria in shallow lakes." *Trends Ecol. Evol.*, 8: 275–279.
- Tanino, Y. and Nepf H.M. (2008). "Laboratory investigation of mean drag in a random array of rigid, emergent cylinders." *J. Hydr. Eng.*, 134: 34–41. DOI: 10.1061/(ASCE)0733-9429(2008)134:1(34).
- Teeter, A.M., Johnson, B.H., Berger, C., Stelling, G., Scheffner, N.W., Garcia, M.H. and Parchure, T.M. (2001) "Hydrodynamic and sediment transport modeling with emphasis on shallow-water, vegetated areas (lakes, reservoirs, estuaries and lagoons)." *Hydrobiologia*, 444, 1–23.
- Thornton, E.B. and Guza, R.T. (1983). "Transformation of wave height distribution." *J. Geophys. Res.*, 88(C10), 5925–5938.
- U.S. Army Coastal Engineering Research Center (1984). "Shore Protection Manual". Washington DC.
- Young, I.R. and Verhagen, L.A. (1996). "The growth of fetch limited waves in water of finite depth. Part 1. Total energy and peak frequency." *Coastal Engineering*, 29: 47–78.

### **Table legends**

Table 1. Depths and distances along the transects at the measurement sites.

Table 2. General characteristics of each measurement cycle at the shallow site

Table 3. General characteristics of each measurement cycle at the deep site.

### **Figure legends**

Fig. 1. Transformed probability density functions (pdfs) with regard to energy dissipation in a reed belt for different values of the parameter  $xBH_{rms}$ . (Rayleigh pdf is assumed for no dissipation.)

Fig. 2. a) Lake Krankesjön, dashed line is the approximate edge of reed vegetation along the shoreline (the depth can change interannually), b) reed vegetation at the deep site.

Fig. 3. Measurement sites including schematic stand density and position of the poles. a) Shallow site, b) deep site.

Fig. 4. Estimated significant wave heights,  $H_s$ , (U.S. Army Coastal Eng. 1984) compared with measured significant wave heights from several measurements taken in the open water for different wind speeds ( $1.7\text{--}8.7\text{ m s}^{-1}$ ) and fetches ( $1.0\text{--}1.4\text{ km}$ ) in Lake Krankesjön.

Fig. 5. Wave damping at the shallow site for every 3-minute measurement period.

Fig. 6. Wave damping at the deep site for every 3-minute measurement period (Pole 2 is excluded since it was not in the vegetation). Grey-filled symbols are for  $H_{rms} < 2$  cm.

Fig. 7. Calculated  $H_{rms}$  inside the reeds compared to measured value. a) Site specific  $C_D$  (rmse=0.3 cm), b) best fit  $C_D$  for both sites together (rmse=0.4 cm). Dotted lines are  $\pm$ rmse.

Fig. 8. Examples of histograms of wave heights at the shallow (2006-07-14) and the deep site (2006-07-06) showing incident waves and waves within the vegetation measured simultaneously. Rayleigh pdf for incident waves are based on  $H_{rms}$  while Rayleigh pdf and transformed pdf for the waves in vegetation are based on calculated  $H_{rms}$  using site specific  $C_D$ .

Fig. 9. Average non-dimensional probability density function with standard deviations for a) shallow site, b) deep site, c) both sites, and d) both sites for  $x > 3$  m and  $H_{rms} > 0.03$  m.

Fig. 10. The drag coefficient,  $C_D$  as a function of a) Reynolds number,  $Re$ , and b) Keulegan-Carpenter number,  $K'$ .

Fig. 11. The drag coefficient  $C_D$  as a function of distance into the reed  $x$  (m), for a) the shallow site, and b) the deep site.

Fig. 12. Wave damping in the reed vegetation for different values of  $C_D$ . For all curves:

$H_{rms0}=0.07$  m,  $d=1$  m,  $D=0.06$  m,  $N=45\text{m}^{-1}$ , and  $T=1.2$  s.

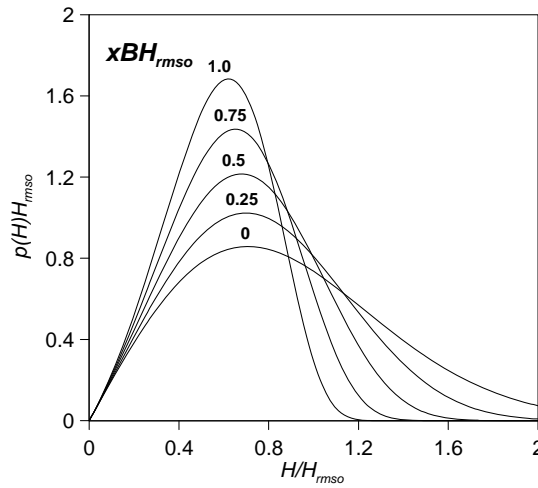


Figure 1.

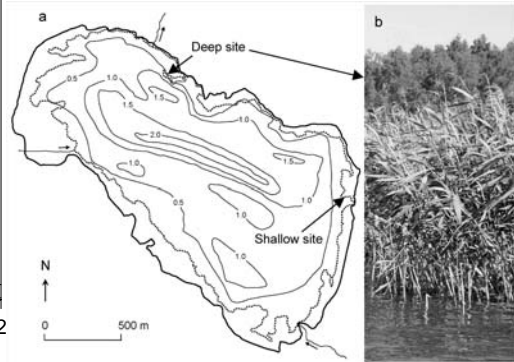


Figure 2.

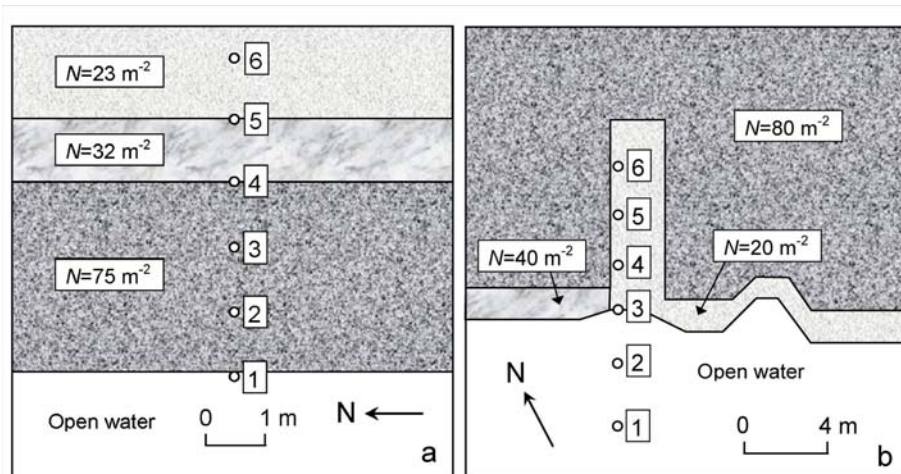


Figure 3.

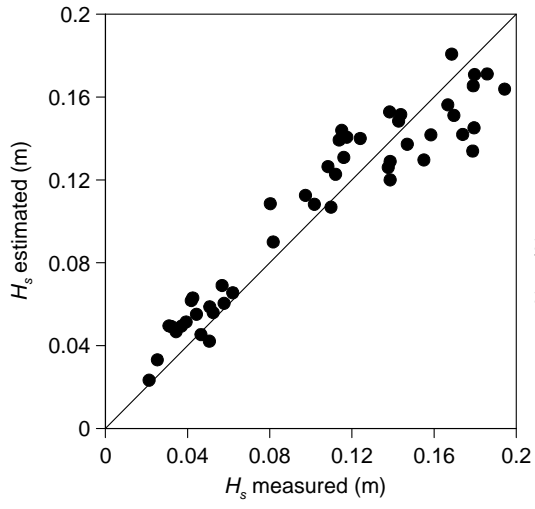


Figure 4.

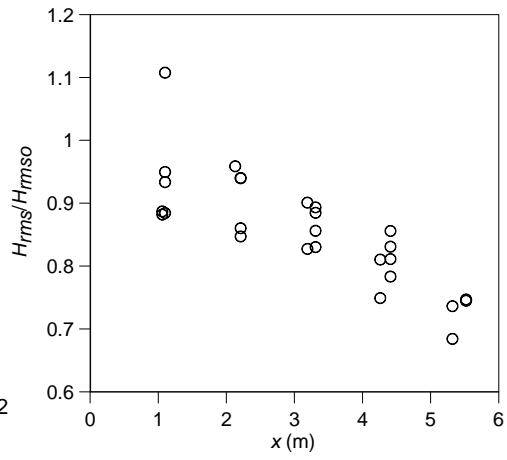


Figure 5.

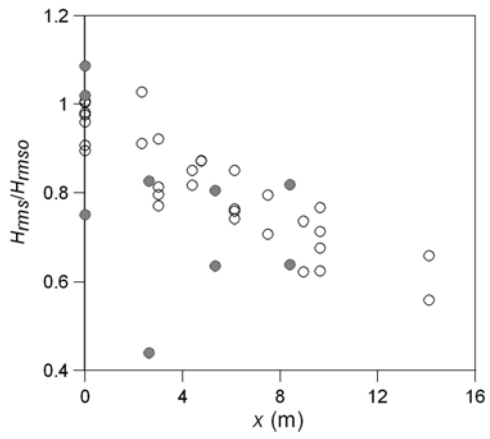


Figure 6.

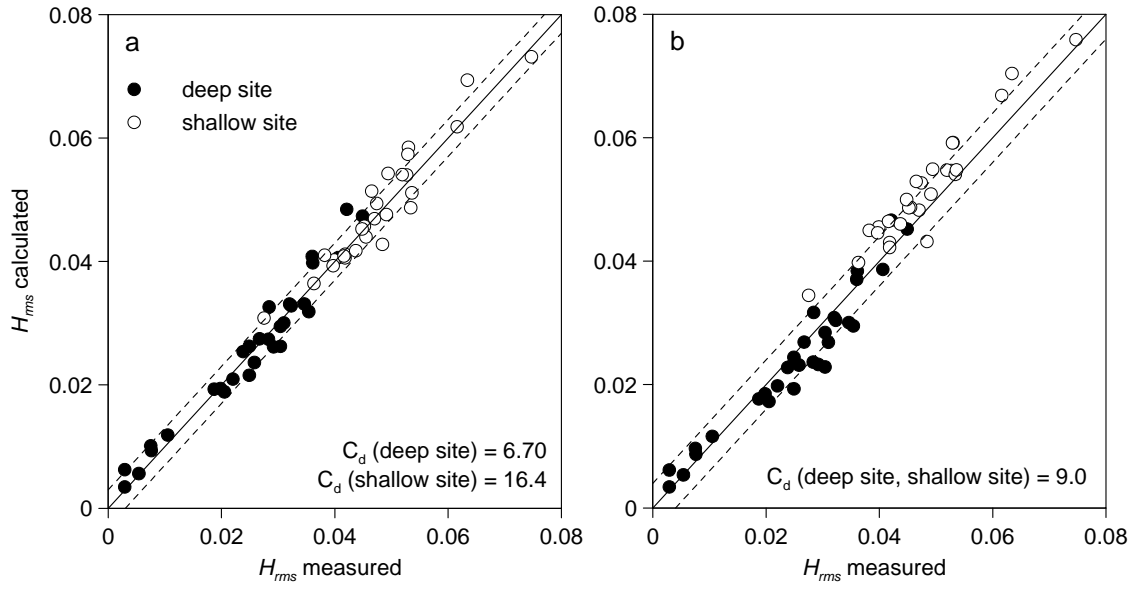


Figure 7.

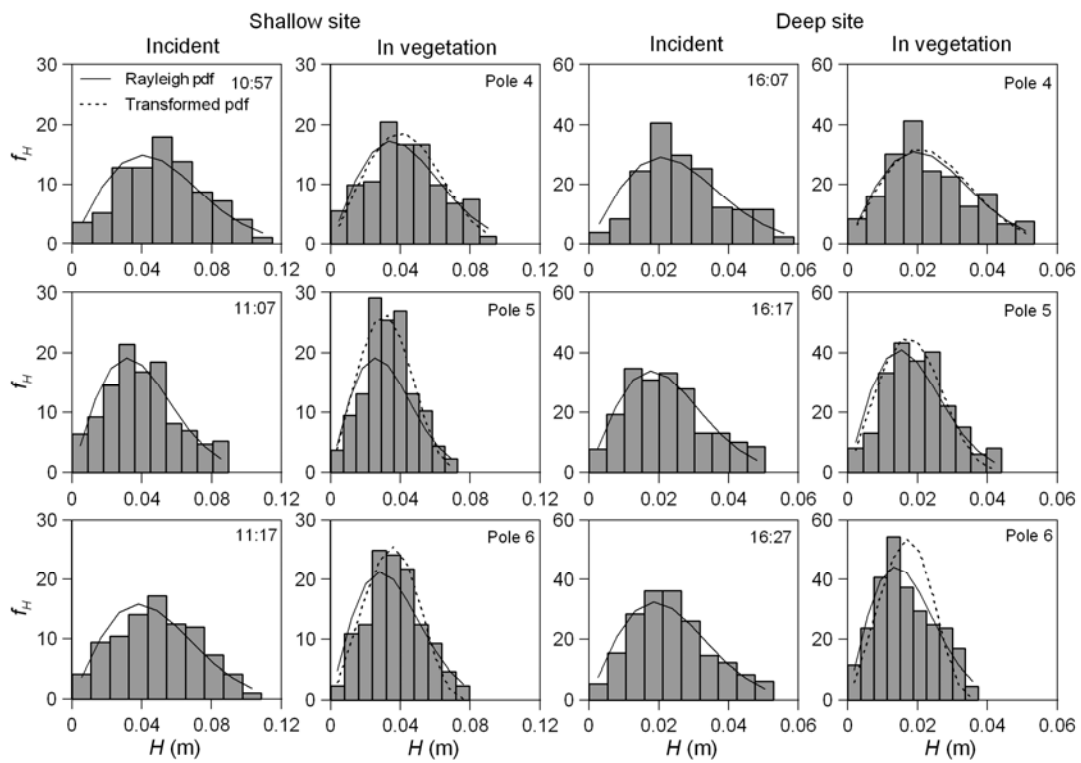


Figure 8.

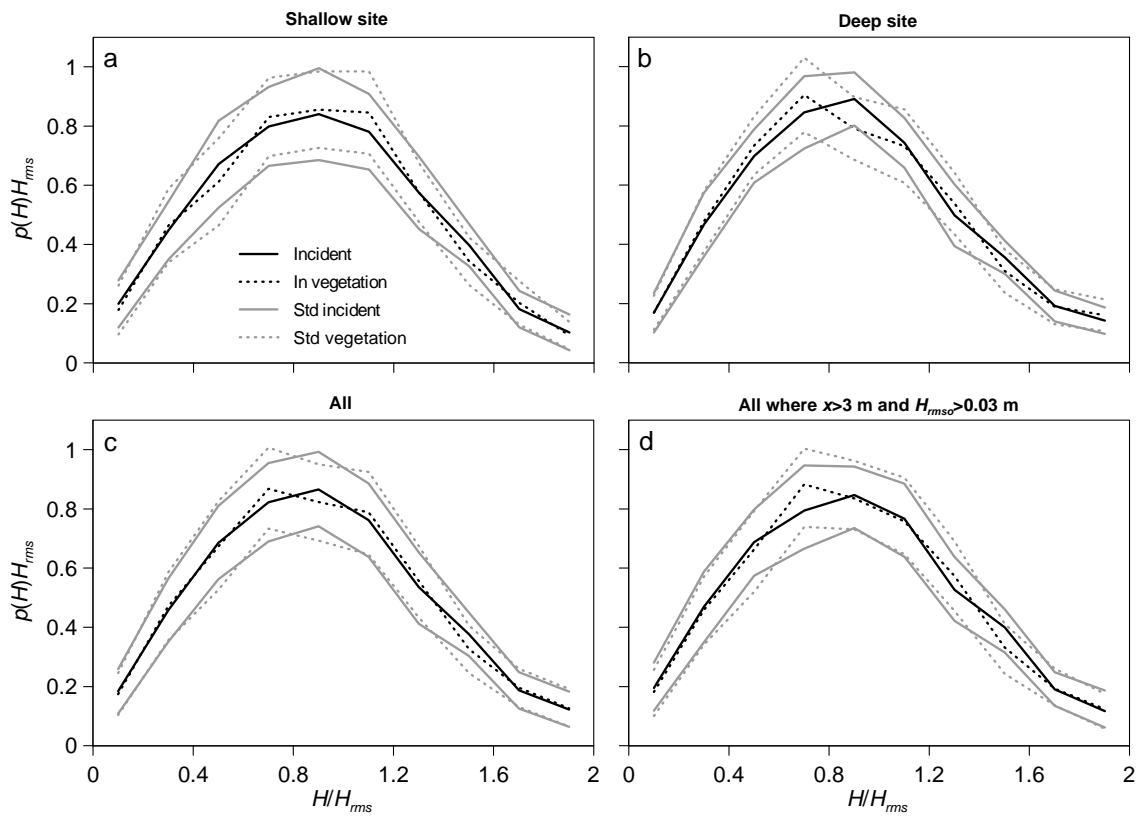


Figure 9.

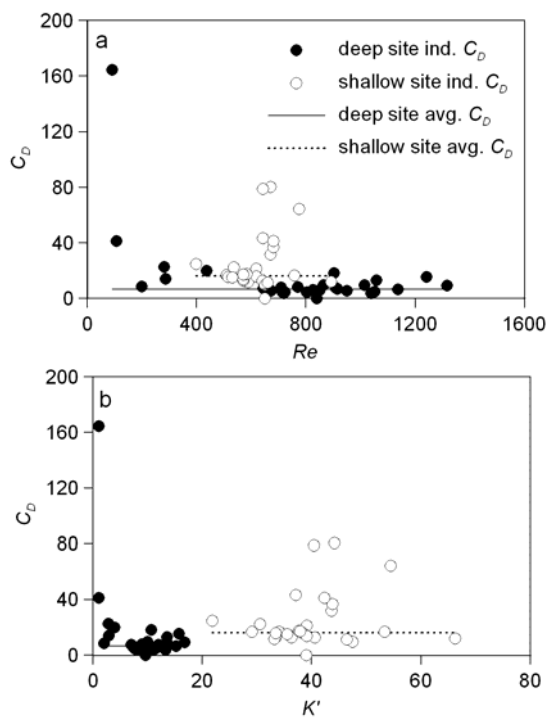


Figure 10.

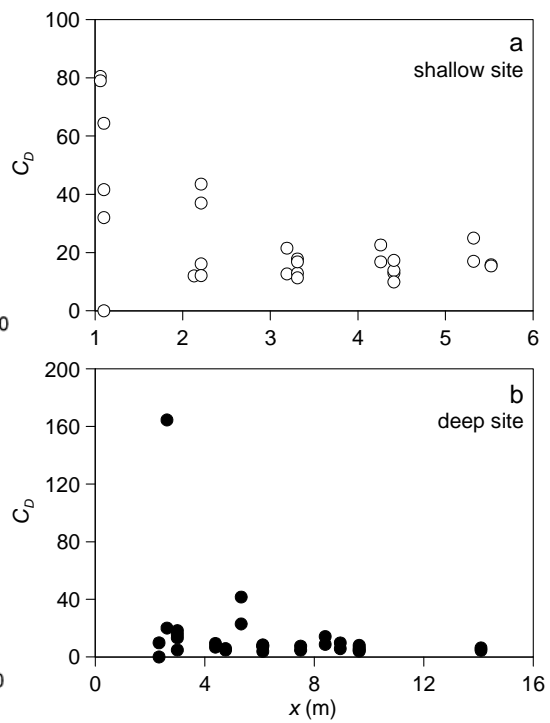


Figure 11.

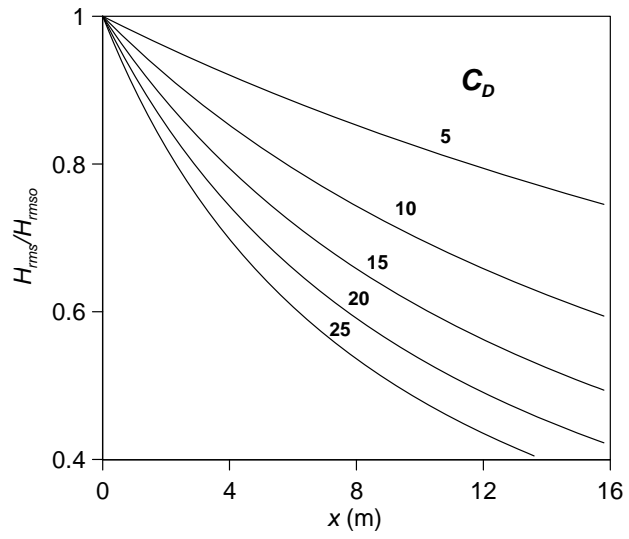


Figure 12.